Supplementary Material

Graphene quantum dot composite with multiphoton excitation as near infrared-II probe in bioimaging

Wen-Shuo Kuo[a,b,#], Yen-Sung Lin[c,d,#], Meng-Zhi Han[c,#], Hao-Yu Chuang[e,f], Ping-Ching Wu[g], Chia-Yuan Chang[h], Jiu-Yao Wang[b], Hui-Fan Kao[i], Shih-Wen Tseng[j], Sheng-Han Lin[k,*], Po-Lan Su[l,*] and Chan-Chi Chang[m,*]

[a]School of Chemistry and Materials Science, Nanjing University of Information Science and Technology, Nanjing 210044, Jiangsu, China

[b]Center for Allergy Immunology and Microbiome (AIM), China Medical University Children's Hospital/China Medical University Hospital, China Medical University, Taichung 404, Taiwan

[c]Division of Pulmonary and Critical Care Medicine, An Nan Hospital, China Medical University, Tainan 709, Taiwan

[d]Department of Nursing, Chung Hwa University of Medical Technology, Tainan 717, Taiwan

[e]Cell Therapy Center / Department of Neurosurgery, An Nan Hospital, China Medical University, Tainan 709, Taiwan

[f]Department of Neurosurgery, China Medical University Beigang Hospital, Yunlin County 651, Taiwan

[g]Department of Biomedical Engineering, National Cheng Kung University, Tainan 701, Taiwan

[h]Department of Mechanical Engineering, National Cheng Kung University, Tainan 701, Taiwan

[i]Department of Nursing, National Tainan Junior College of Nursing, Tainan 700, Taiwan

[j]Core Facility Center of National Cheng Kung University, National Cheng Kung University, Tainan 701, Taiwan

[k]Department of Anesthesiology, E-Da Hospital, Kaohsiung 824, Taiwan

[l]Department of Internal Medicine, National Cheng Kung University Hospital, College of Medicine, National Cheng Kung University, Tainan 701,Taiwan

[m]Department of Otolaryngology, National Cheng Kung University Hospital, College of Medicine, National Cheng Kung University, Tainan 701,Taiwan

[#]The authors contributed equally to this work.

*To whom correspondence should be addressed. E-mail: ed111667@edah.org.tw (S.H. Lin), polan.750317@gmail.com (P. L. Su) and 109a0015@gs.ncku.edu.tw (C.C. Chang)

Materials and Methods

Preparation of graphene quantum dot (GQD)–based materials (Hummers et al., 1958)

GQDs: Graphene oxide was prepared using a natural graphite powder (Bay Carbon Inc., Bay City, MI, USA) through a modified Hummers' method (Hummers et al., 1958). Graphite (8.5 M) and $NaNO_3$ (0.6 M) (Merck & Co., Kenilworth, NJ, USA) were mixed with H_2SO_4 (FUJIFILM Wako Chemicals USA Inc., Richmond, VA, USA). $KMnO_4$ (2.0 M, FUJIFILM Wako Chemicals USA Inc.) was slowly added with continual stirring at 35°C (Corning, New York, NY, USA) overnight. Subsequently, deionized water (ddH_2O) was gradually added and continually stirred before H_2O_2 (35%; Sigma Aldrich Co., St Louis, MO, USA) was added to terminate the reaction. The graphene oxide was washed several times with ddH_2O before it was collected and placed in a tube furnace (Tainan, Taiwan) and heated to 400–600°C in the presence of argon for 4–6 h. Concentrated HNO_3 (16.0 M, Sigma Aldrich Co.) was added and stirred for 2 d. The mixture was placed in a water bath sonicator (Rocker Scientific Co. Ltd., New Taipei City, Taiwan) for 2 d at 45°, then placed in an oven at 160°C (Yotec Instruments Co. Ltd., Hsinchu City, Taiwan) for 1 d to vaporize all the liquid. Washing and centrifugation (approximately 847200 RCF, > 10 min; Optima TLX Ultracentrifuge, Beckman Coulter Inc., Brea, CA, USA) with ddH_2O were conducted several times before the supernatant was filtered through a 0.22 μm microporous membrane (Nylon filter membrane, Merck & Co.). The pH (7.4; Hanna Co. Ltd., Thane, Maharashtra, India) of the resulting black suspension was adjusted with NaOH (Sigma Aldrich Co.) to obtain the GQDs specimens.

GQDs doped with nitrogen (N-GQDs): Graphene oxide was prepared from a natural graphite powder using a modified Hummers' method. Graphite (8.5 M) and $NaNO_3$ (0.6 M) were mixed with H_2SO_4 and $KMnO_4$ was slowly added with continual stirring at 35°C overnight. Subsequently, ddH_2O was gradually added and continually stirred before the reaction was terminated with H_2O_2. Several washing and centrifugation steps with ddH_2O were performed and the graphene oxide was collected. The as-prepared graphene oxide was placed in a tube furnace and heated to 400–600 °C in the presence of ammonia (Sigma Aldrich Co.) for 4–6 h before the addition of concentrated HNO_3 (16.0 M) and stirred for 2 d. The mixture was placed in a water bath sonicator for 2 d at 45°C, then placed in an oven at 160°C for 1 d to vaporize all the liquid. Washing and centrifugation (approximately 847200 RCF, > 10 min) with ddH_2O were performed several times before the supernatant was filtered through a 0.22 μm microporous membrane. The pH (7.4) of the resulting black suspension was adjusted with NaOH to obtain the N-GQDs.

GQDs doped with N and functionalized with amino groups (amino-N-GQDs): The as-prepared N-GQDs were mixed with ammonia, stored in a Teflon-lined stainless steel autoclave, and reacted at 180°C for 5 h. The resulting mixture was washed with ddH_2O, centrifuged several times, and subsequently dried in an oven at 50°C overnight to obtain the amino-N-GQDs.

The 0.1 mg mL^{-1} or 1.0 mg mL^{-1} stock solution of materials was prepared for the following experiments.

Synthesis and characterization of amino-N-GQDs coated with polymer materials [amino-N-GQD-polystyrene sulfonate (PSS)-polyethylenimine (PEI) or amino-N-GQD-polymer

composites)]

Both negatively charged PSS and positively charged PEI (both 50 μg mL^{-1}; Sigma Aldrich Co., St Louis, MO, USA) were coated on the surface of as-prepared positively charged amino-N-GQDs (50 μg mL^{-1}) through electrostatic interaction to form amino-N-GQD-PSS-PEI (or amino-N-GQD-polymer composites). The solutions were centrifuged (approximately 847200 RCF, > 10 min) for 20 min to remove excess polymers. The pellets (amino-N-GQD-PSS-PEI or amino-N-GQD-polymer composites) were resuspended in ddH_2O, and the centrifugation process was repeated several times to obtain the amino-N-GQD-polymer composites specimens.

Characterization

Materials were subject to transmission electron microscopy (TEM, JEOL 2100F and JEOL 3010, Akishima, Tokyo, Japan) observation. Fourier-transform infrared spectroscopy (FTIR), Ultraviolet-visible (UV-Vis) spectroscopy, X-ray diffraction (XRD) and zeta potential spectra/dynamic light scattering (DLS) of samples were recorded by the spectrometers: Bruker AXS Gmbh, D2 Phaser, Billerica, MA, USA; RX1, PerkinElmer, Waltham, MA, USA; U-4100 Hitachi, Chiyoda-ku, Tokyo; and Malvern Nano-ZS90, Worcestershire, West Midlands, UK, respectively. The height profile diagram, thickness and size of samples were determined by atomic force microscopy (AFM, multimode 8, Bruker, Billerica, MA, USA). Raman spectroscopy (DXR, Thermo Scientific, Waltham, MA, USA) was used to examine the crystallinity of samples with 532 nm laser. X-ray photoelectron spectroscopy (XPS, PHI VersaProbe 4, Chanhassen, MN, USA) was employed to examine the surface chemistry of the materials, the O(1s)/C(1s) and N(1s)/C(1s) atomic ratios of materials. The PL signal was recorded by the spectrophotometer (F-7000, Hitachi, Chiyoda-ku, Tokyo, Japan).

XPS for amino-N-GQDs

For amino-N-GQDs: C–C/C=C (285.8 eV), C–N (286.8 eV), C–O (287.2 eV) and C=O (288.1 eV). The C–O bonds were identified as corresponding to functional groups of epoxy and tertiary alcohol on the basal plane as well as phenol and ether groups located at the graphene sheet's periphery. The C=O bond indicated the presence of carbonyl group at the graphene periphery. The contribution of the C–N bonds was increased at the expense of those of the C–O and C＝O bonds through ammonia treatment. This indicated that the epoxy and carbonyl groups were converted in the treatment. The deconvoluted N(1s) spectrum of the amino-N-GQDs provides further details of the C–N bonding, and it is indicated that the ammonia-treated samples contained pyridinic (398.2 eV), amino (398.9 eV), pyrrolic (399.8 eV), quaternary (400.8 eV), and amide (O=C–N, 401.2 eV) nitrogen-containing functional groups. Derived from the deconvoluted N(1s) spectra, the nitrogen functionality compositions indicated that the hydrothermal ammonia treatment resulted in considerable nitrogen atom doping and led to the formation of pyridinic, pyrrolic, and quaternary nitrogen functionalities. Some proportions of epoxy and carbonyl groups were also discovered to have been converted; they respectively formed amino and amide functionalities (**Figs. 1d-e**). Nitrogen functionalities are known to strongly affect the resonance patterns of electron orbitals in all

materials based on graphene oxide. The annealing ammonia treatment may have caused aromatic ring damage and the formation of defective pyrrolic and carbonyl groups at the periphery as the graphene oxide treated with ammonia was ultrasonically exfoliated and cut in nitric acids. The subsequent hydrothermal ammonia treatment of the produced N-GQDs caused conversion of the carbonyl groups to amide groups on amino-N-GQDs. The corresponding conceptual schematic of the amino-N-GQD is shown in **Fig. S1f**.

Estimating the amount of polymers per material

The absorbance of a certain quantity of PSS or PEI was recorded via UV-Vis spectroscopy (Abs: approximately 217 nm and 252 nm for PSS; approximately 214 nm for PEI) (**Fig. S6**). By electrostatic interaction, the materials were mixed with the same quantity polymers for 30 min during incubation at room temperature in the dark and centrifuged (approximately 847200 RCF, > 10 min) to remove excess polymers; the amino-N-GQD-PSS and amino-N-GQD-PSS-PEI were then prepared. Conversely, the supernatant the amino-N-GQD-PSS and amino-N-GQD-PSS-PEI were retained and its absorbance was measured. The difference between the absorbance of the collected supernatant and the polymers were estimated. Consequently, the quantity of the antibody absorbed on the materials was calculated using Lambert-Beer's law [$A = \varepsilon bC$, where A= absorbance, ε= molar extinction coefficient, b= path length (1 cm), and C= concentration] (**Fig. S6**).

Coating antibodies

The absorbance of a certain quantity of antiepidermal growth factor receptor antibody (Ab_{EGFR}; abcam, Cambridge, UK) was recorded via UV-Vis spectroscopy (Abs: approximately 216 nm and 272 nm) (**Fig. S10**). By electrostatic interaction, the materials were mixed with the same quantity antibody for 30 min during incubation at 4 ℃ in the dark and centrifuged (approximately 847200 RCF, > 10 min) to remove excess antibody; the material-Ab_{EGFR} was then prepared. Conversely, the supernatant was retained and its absorbance was measured. The difference between the absorbance of the collected supernatant and the original antibody was estimated. Consequently, the quantity of the antibody absorbed on the materials was calculated using Lambert-Beer's law [$A = \varepsilon bC$, where A= absorbance, ε= molar extinction coefficient, b= path length (1 cm), and C= concentration] (**Fig. S10**). Besides, the zeta potential was also used to characterize the coating of material-Ab [The parameters of zeta potential were as follows. Cell type: DTS1060C; Measurement duration: 30 number of runs, 20 run duration (sec). Delivered dose: 1.0 mg mL^{-1} material] and the results were as follows. Eventually, the material-Ab_{EGFR} was then well prepared. In the culture medium of human squamous carcinoma cell line (A431 skin cancer cells), approximately 0.88 μg of Ab_{EGFR} was absorbed on 10 μg of amino-N-GQD-polymer composites. This implies that the absorption efficiency of the culture medium of A431 cancer cells was approximately 8.8% (zeta potential of amino-N-GQD-polymer composites-Ab_{EGFR} : 12.6 eV). For amino-N-GQD-Ab_{EGFR}, the efficiency of absorption was approximately 9.1% (13.3 mV of zeta potential) in the culture medium of A431 cancer cells. Moreover, the positively charged material-Ab was favorable for absorbance or internalization by the negatively charged cell surface. The aforementioned results have proven the successful absorption of Ab on

the surface of materials**.**

Cell culture of A431 skin cancer cells and MTT assay

A431 cells were cultured in EMEM (EBSS) + 2mM Glutamine + 1% Non Essential Amino Acids + 10% Fetal Bovine Serum at 37℃ under 5% CO_2 in air. The cells were collected by trypsinization and placed onto a 10 cm tissue culture Petri dish, then allowed to grow for 2-4 days. For MTT assay, cells (5×10^3 per well in a 96-well culture plate) were incubated overnight and then treated with material-Ab_{EGFR} for 24 h incubation in an incubator (37 ℃). The culture medium was removed and replaced with the new culture medium containing. Repeat for 3 to 5 times to wash out the nonspecific binding. MTT reagents (10%) (Sigma-Aldrich, St. Louis, MO, USA) followed by incubation for 4 h at 37 ℃, leading to the formation of formazan dye. The medium was then changed with dimethyl sulfoxide (DMSO, 200.0 μL; Fisher Scientific, Hampton, NH, USA) for 10 min, followed by centrifugation at 4000 rpm for 10 min. The supernatant was transferred into a new ELISA plate and the absorbance was measured at A540 with an ELISA reader (Thermo Scientific, Waltham, MA, USA).

Quantum yield (QY) measurement (Li et al., 2012, Umezawa et al., 2009)

The relative PL QY of contrast agent is usually the ratio of the emitted photons to the absorbed photons and is given as follows:

$$QY = QY_{ref}\,(\eta^2/\eta_{ref}^2)(I/A)(A_{ref}/I_{ref})$$

(Equation S1)

, where QY_{ref} =0.28 is the QY of Cy5.5 dissolved in dimethyl sulfoxide (DMSO; Sigma-Aldrich, St. Louis, MO, USA) as a reference, η is the refractive index of ddH_2O=1.33 (η_{ref} of DMSO=1.48), I is the integrated fluorescence intensity and A is the absorbance at the excitation wavelength. OPE or TPE yields the same QY.

Femtosecond laser optical system for the measurements of two-photon absorption (TPA) and two-photon luminescence (TPL) (Kuo et al., 2010)

The self-made femtosecond Ti-sapphire laser optical system (a repetition rate of 80 MHz; Mai Tai with the optical parametric oscillators, Spectra-Physics, CA, USA; **Scheme S1**): an inverted optical microscope (Axiovert 200, Zeiss, Oberkochen, Germany), a *x*-*y* galvanometer scanner (6215H, Cambridge, MA, USA), a triple-axis sample-positioning stage (ProScan™II, Prior Scientific Instruments Ltd., Cambridge, UK), a *z*-axis piezoelectric nano-positioning stage (Nano-F100, Mad City Labs, Madison, WI, USA), photomultiplier tubes (Hamamatsu, Shizuoka Prefecture, Japan), and a data acquisition card with a field-programmable gate array module (National Instruments, Austin, TX, USA). **TPA measurement.** A femtosecond laser was used to excite TPA signals. A time-average luminescence photon count (F) is proportional to the cross section (δ) of TPA and can be given as

$$F \approx \frac{1}{2}\delta\eta_2\phi C\frac{g_p}{f\tau}\frac{8nP^2}{\pi\lambda},$$

(Equation S2)

where C the concentration of the photoinitiator (concentration: the aqueous material was put in oven overnight to vaporize the whole liquid and weighed it. Sequentially, the dry materials can be dissolved in any applicable amount of working solution), η_2 is the quantum efficiency of photoluminescence, ϕ the luminescence collection efficiency of the system, P the average incident power, g_p the dimensionless quantity for degree of the second-order temporal coherence, f the pulse repetition rate, n the refractive index of the measurement medium, λ the excitation wavelength and τ the excitation pulse width by full-width at half maximum. After the SF-10 prism pair compensation, the parameters which are the collection system, the pulse repetition rate, the concentration of the materials and the excitation power can be maintained the same at different excitation wavelengths with their corresponding excitation pulse widths. On the basis of the measured excitation pulse width, the measured fluorescence photon count and the excitation wavelength, the TPA was derived as $\delta \times \eta_2$. *Via* the SPC module, the photomultiplier tubes were used to collect the PL photon The TPA can be given as

$$\delta\eta_2 \propto \lambda\tau F. \qquad \text{(Equation S3)}$$

with a galvanometer scanner speed of 2 m ms^{-1}, the excitation spectrum was measured as 900-1000 nm with an excitation power of 2.0 mW [this is the power before objective; the power after objective (or on sample) is 1.1832 mW or 118.32 nJ pixel^{-1}]. Therefore, the relative TPA spectrum as function of excitation wavelength for the amino-N-GQD and amino-N-GQD-polymer composites was measured and shown in **Fig. S8a** and **Fig. 2b**, respectively. **Measurement of TPL spectrum.** The material was exposed to TPE from the femtosecond laser at an excitation wavelength of 980 nm, a power of 159.32 nJ pixel^{-1} (1.5932 mW), a scanning area of 200 × 200 μm, a frequency of 10 kHz, an exposure time of 1.638 s/(scan, pixel)= 100 μs, 128 × 128 pixels/scan, and a pixel area of 1562.5 nm× 1562.5 nm. The focal spot area was calculated as $\pi d^2/4$, where d= 0.61 λ/numerical aperture (*NA*) is the full width at half maximum of the beam waist. For instance, at the *x*–*y* axis focal spot with 980 nm excitation and a 40× oil-immersion objective with an *NA* of 1.3, d= 0.61 × 980 nm/1.3= approximately 459.85 nm, and the *z*-axis resolution (full width at half maximum) was measured to be 0.94835 μm= 948.35 nm (**Fig. 2a**). For 980 nm excitation, the exposure time per scan for an individual nanomaterial is expressed as (focal spot area/pixel area) × 100= approximately 6.80 ms, and the total exposure time t= 6.80 ms × number of scans. A 40× oil-immersion objective (*NA* 1.3) was used to collect the signals, and the detection range of the spectrum photometer was 500-900 nm.

Additionally, the calculations of laser power (mW or J pixel^{-1}) used on the sample were as follows. For the 40× oil-immersion objective (*NA* 1.3), the transmission rate at 980 nm in wavelength is approximately 68% in this optical system, and the laser power went from the output to the objective with approximately 87% of the original output power due to the loss of power. As a result, the calculated energy after the objective (on sample) is P_{output}(mW)*68%*87%= approximately 0.5916*P_{output} (mW). For instance, P_{output}= 2.0 mW, the calculated energy after the objective (on the sample) is 2.0 mW*68%*87%= 1.1832 mW. With 10 kHz of scan rate (each pulse stays 0.1 ms pixel^{-1}), the calculated energy on the sample (J pixel^{-1}) was around P_{output} (mW)*68%*87%*0.1 ms= approximately 0.05916*P_{output} (J pixel^{-1}). For instance, P_{output}= 2.0

mW, the energy (J pixel^{-1}) on sample= 2.0 mW*68%*87%*0.1 ms= 0.11832 μJ pixel^{-1}= 118.32 nJ pixel^{-1}. The power after the objective (on the sample) was used and marked throughput this manuscript.

Measurement of TPE absolute cross section (Kuo et al., 2016, Kuo et al., 2022, Horton et al., 2013, Li et al., 2020, Ouzounov et al., 2017, Wang et al., 2005, Xu et al., 1996)

The absolute cross section of TPE was measured on the basis of luminescence signals by using the home-made femtosecond Ti-sapphire laser optical system, as described above (**Scheme S1**). A 40× oil-immersion objective (*NA* 1.3) was overfilled by expansion of the laser beams. For the multiphoton excitation, the diffraction-limited illumination of the sample was approximately achieved and analyzed. Under TPE and for the thick sample limit, the relation between time-averaged luminescence photon flux$\langle F^{(n)}(t)\rangle$ and the incident power *P(t)* can be obtained. The formula can be given as,

$$\langle F^{(n)}(t)\rangle = \frac{1}{n}\frac{g_p^{(n)}}{(f\tau)^{n-1}}\phi\eta\sigma_n C n_0 \frac{a_n(\mathrm{NA})^{2n-4}\langle P(t)\rangle^n}{8\pi^{3-n}\lambda^{2n-3}}$$

(Equation S4)

, where C is the concentration of the fluorophore (concentration: the aqueous material was put in oven overnight to vaporize the whole liquid and weighed it. Sequentially, the dry materials can be dissolved in any applicable amount of working solution), n is the number of photons absorbed (n = 2 for the TPE), ϕ is the system collection efficiency, τ is the laser pulse width, f is the laser repetition rate, η is the luminescence quantum efficiency (or quantum yield, QY), and λ is the excitation wavelength in vacuum, σ_n is the n-photon excitation cross section, and a_2 = 64 for TPE. $g_p^{(n)}$ is the n^{th}-order temporal coherence of the excitation source. Due to the limitation of resource we currently have, $\langle F^{(n)}(t)\rangle$ is temporarily not able to be calculated and the values could be replaced by the integrated TPL intensity with the symbol "counts". As a result, the equation for action cross section ($\eta\sigma_2$) is turned into,

$$\eta\sigma_2 = \frac{\text{counts}}{\frac{1}{2}\frac{g_p^{(2)}}{f_\tau} n_0 \phi C \frac{8\langle P(t)\rangle^2}{\pi\lambda}}$$

(Equation S5)

If it was with the same 2^{nd}-order temporal coherence of the excitation source, the laser pulse width, laser repetition rate, incident power, system collection efficiency, wavelength and working concentration, the action cross section of TPE ($\eta\sigma_2$) for a fluorophore as the reference compound is determined relative to the known action cross section, then the Equation S5 is simplified as,

$$(\eta\sigma_2)_2 = \frac{\text{counts}_2}{\text{counts}_1}(\eta\sigma_2)_1$$

(Equation S6)

, where Sample 1 means the reference compound, and Sample 2 means the fluorophore.

The absolute cross section of TPE was measured on the basis of luminescence signals by using a femtosecond laser optical system, as described by the previous studies. The TPL of fluorescein and

Rhodamine B (Sigma Aldrich Co., USA) had to be verified. The results are shown in **Fig. S9** and were obtained by measuring the dependence of the emission intensity with an excitation power range of 1183.2 nJ pixel^{-1} (11.832 mW) to 4732.8 nJ pixel^{-1} (47.328 mW). Quadratic dependence with the exponents of approximately 2.01 for fluorescein and approximately 2.03 for Rhodamine B was measured for increasing the excitation power to determine the luminescence from TPE. According to the previous studies, the action cross sections of TPE for fluorescein and Rhodamine B are 16.32 and 19.20 Göeppert–Mayer units (GM; 1 GM = 10^{-50} cm^{4}s photon^{-1}), respectively, for 980 nm excitation. We also referred to the free website http://www.drbio.cornell.edu/cross_sections.html, kindly provided by Prof. Chris Xu (Cornell University, NY, USA). The TPE action cross sections for fluorescein and Rhodamine B were calculated to be 15.83 and 20.01 GM, respectively (**Table S1**), which indicated an error of less than 5% compared with those from Prof. Xu's laboratory. In this study, Rhodamine B was chosen as the standard reference for determining the cross section, and the calculated absolute cross sections of TPE for the amino-N-GQD and amino-N-GQD-polymer composites were approximately 51031 GM and 60158 GM, respectively. The measured parameters for calculating the TPE absolute cross sections of samples are shown in **Table 1**. Additionally, the calculated absolute cross sections of TPE for the sorted dots were also calculated by using Fluorescein as the standard reference. Results show that the value of cross section (amino-N-GQD: ~51721 GM; amino-N-GQD-polymer composites: ~60579 GM) was less than only 1.4% of difference between chosen Rhodamine B and Fluorescein (**Table S6**). No batch-to-batch variation was observed for the materials in two-photon properties, two-photon photodynamic ability, and two-photon contrast agents.

Femtosecond laser optical system (for fluorescence lifetime imaging microscopy, FLIM) (Ouzounov et al., 2017, Xu et al., 1996**)**

The self-made femtosecond Ti-sapphire laser optical system mentioned above was used (**Scheme S1**). For FLIM, the time-correlated single photon counting (TCSPC) module (PicoQuant, Germany) is integrated into the main control platform based on LabVIEW programming, which triggers the synchronic signal through the FPGA module, collects the fluorescence time-to-digital data via a USB interface, and then constructs the fluorescence lifetime image by using LabVIEW. The time-to-digital data from different pixels are separated by inserting a marker signal from scanning synchronic trigger. To facilitate a three-dimensional (3D) lifetime image and data analysis, the LabVIEW program also records scanning parameters corresponding to the time-to-digital data. The timer overflow signal of the TCSPC is removed, allowing the accumulated time-to-digital data of each pixel to form a histogram. A nonlinear least square algorithm is used to fit the fluorescence lifetime decay curve for each pixel. In accordance with the fitting lifetime data of each pixel and the pixel scanning information, the FLIM image can be displayed with a resolution of 0.1 ns under the main control platform. The lifetime data and parameter are generated using the triple-exponential equation fitting [3 exp fitting model: a0*exp(a1x)+a2*exp(a3x)+a4*exp(a5x)+a6] while monitoring the emission under TPE (Ex: 980 nm) (**Table 2**).

$$t_{average} = \frac{1}{a_0 + a_1 + a_4}(a_0 \cdot t_1 + a_2 \cdot t_2 + a_3 \cdot t_3) \quad \text{(Equation S7)}$$

$t_{average}$: average lifetime, t_1: lifetime1, t_2: lifetime2, t_3: lifetime3

Calculation of radiative and non-radiative decay rates (Kuo et al., 2016, Lakowicz et al., 2006, Suhling et al., 2015)

PL QY and lifetime are both major parameters when investigating the emission characteristics of fluorescent dyes in diverse environments. The quantum yield (Q) can be expressed as follows:

$$Q = \frac{\Gamma}{\Gamma + k} \qquad \text{(Equation S8)}$$

, where Γ is the radiative decay rate and *k* is the nonradiative decay rate.

Fluorescence lifetime is usually defined as the average time required for an electron in the excited state to decay to the ground state. The TPL lifetime τ can also be relative to the decay rates and is described as follows:

$$\tau = \frac{1}{\Gamma + k} \qquad \text{(Equation S9)}$$

Following Equations (S8-S9), the radiative and nonradiative decay rates can be calculated.

Upon the absorption of a photon, one of the weakly bound electrons of the fluorescent molecule—a fluorophore—is promoted to a higher energy level. The fluorophore is then in an excited state, *A**. This state is metastable; therefore the fluorophore will return to its stable ground state, *A*. It can do so either radiatively by emitting a fluorescence photon *hv*,

$$A^* \; -> \; A + hv$$

or nonradiatively, by dissipating the excited state energy as heat

$$A^* \; -> \; A + \text{heat}$$

The depopulation of the excited state depends on the de-excitation pathways available. Fluorescence is radiative deactivation of the lowest vibrational energy level of the first electronically excited singlet state, S_1, back to the electronic ground state, S_0. The singlet states are the energy levels that can be populated by the weakly bound electron without a spin flip. The absorption and emission processes are illustrated by an energy level diagram named after Aleksander Jablonski.

The fluorescence lifetime, τ, is the average time a fluorophore remains in the electronically excited state S_1 after excitation. τ is defined as the inverse of the sum of the rate parameters for all excited state depopulation processes: Eqs. (S8-S9), where the nonradiative rate constant *k* is the sum of the rate constant for internal conversion, k_{ic}, and the rate constant for intersystem crossing to the triplet state, k_{isc}, such that $k = k_{ic} + k_{isc}$. Fluorescence emission always occurs from the lowest vibrational level of S_1, a rule known as the Kasha's rule, indicating that the fluorophore has no memory of its excitation pathway, for example, OPE and TPE yield the same fluorescence spectrum, QY and lifetime.

Uptake assay

A431 cells were incubated with 3 μg mL^{-1} material-Ab_{EGFR}. The absorbance of 3 μg mL^{-1} material-Ab was recorded using UV-Vis spectroscopy (Abs: approximately 216 nm). The material-Ab_{EGFR} was mixed with A431 cells at 37 ℃ from 1 h to 10 h, respectively. Then, the mixture was centrifuged (1200 rpm) to remove excess materials, keep the supernatant, and measure the absorbance of the supernatant. The difference between the absorbance values of the collected supernatant and the original materials was estimated, thus resulting in the percentage of uptake at each time point. Data are presented as mean ± SD (n=6).

Reactive oxygen species (ROS) detection (Kinen et al., 2000, Kuo et al., 2016, Kuo et al., 2017, Possel et al., 1997)

Singlet oxygen ($^1O_2$): (a) materials (1 or 10 μg mL^{-1}) were exposed to TPE photoexcitation [4732.80 nJ $pixel^{-1}$; 6 min (number of scans: approximately 52941 scans); Ex: 980 nm]. ROS were neutralized using 30 ppm of antioxidant α-tocopherol/methyl linoleate (Sigma-Aldrich, St. Louis, MO, USA) added in darkness. Then, Singlet Oxygen Sensor Green (SOSG) reagent (1 μM; Thermo Fisher Scientific, Waltham, MA, USA) (Ex/Em: 488/525 nm) was then added in darkness. Material-Ab (1 or 10 μg mL^{-1}) was treated with A431 cells, after which it was subjected to 3 h of incubation at 37 °C in darkness. Subsequently, the mixture was photoexcited directly; photoexcited with the same treatment (with the previously described ROS neutralization); incubated for 3 h at 37 °C in darkness, and finally mixed with SOSG Reagent. A fluorescence spectrometer was employed for measurements. (b) Materials (1 or 10 μg mL^{-1}) were exposed to TPE photoexcitation [4732.80 nJ $pixel^{-1}$; 6 min (number of scans: approximately 52941 scans); Ex: 980 nm] (with the previously described ROS neutralization), after which 10 μM of trans-1-(2′-methoxyvinyl)pyrene (*t*-MVP) (Thermo Fisher Scientific, Waltham, MA, USA)/0.10 M SDS (Sigma-Aldrich, St. Louis, MO, USA) (Ex/Em: 352/465 nm) was added in darkness. Reaction of *t*-MVP with $^1O_2$ yields a dioxetane intermediate that fluoresces while it decomposes into 1-pyrenecarboxaldehyde. Furthermore, this highly selective fluorescent probe does not react with other activated oxygen species such as hydroxyl radicals, superoxide, or hydrogen peroxide. However, material-Ab (1 or 10 μg mL^{-1}) was respectively treated with A431 cells and then subjected to 3 h of incubation at 37 °C in darkness. After incubation, the mixture was photoexcited directly; photoexcited with the same treatment (with the previously described ROS neutralization); incubated for 3 h at 37 °C in darkness; and mixed with *t*-MVP/0.1 M SDS. A fluorescence spectrometer was employed for measurements. **Superoxide radical anion ($O_2^{\cdot-}$):** materials (1 or 10 μg mL^{-1}) were exposed to TPE photoexcitation [4732.80 nJ $pixel^{-1}$; 6 min (number of scans: approximately 52941 scans); Ex: 980 nm] (with the previously described ROS neutralization), after which 2,3-bis (2-methoxy-4-nitro-5-sulfophenyl)-2H-tetrazolium-5-carboxanilide (XTT) (0.45 mM; Sigma-Aldrich, St. Louis, MO, USA) was added in darkness. The purpose of this material was that it interacted with $O_2^{\cdot-}$ and produced XTT-formazan, resulting in strong absorption (470 nm in wavelength). A UV-vis spectrometer was employed to monitor this absorption. However, material-Ab (1 or

10 μg mL^{-1}) was respectively treated with A431 cells and then subjected to 3 h of incubation at 37 °C in darkness. Subsequently, this mixture was photoexcited (with the previously described ROS neutralization); photoexcited with the same treatment; subjected to 3 h of incubation at 37 °C in darkness; and mixed with XTT. As stated, the signals were recorded using a UV-Vis spectrometer. (b) Materials (1 or 10 μg mL^{-1}) were exposed to TPE photoexcitation [4732.80 nJ $pixel^{-1}$; 6 min (number of scans: approximately 52941 scans); Ex: 980 nm] (with the previously described ROS neutralization), and 50 mM bicarbonate buffer (pH 8.60) and glutathione (*γ*-L-glutamyl-L-cysteinyl-glycine, GSH) (Sigma-Aldrich, St. Louis, MO, USA)/0.80 mM bicarbonate buffer (the Ellman's assay for $O_2^{\cdot -}$ detection) was added in darkness for incubation lasting 3 h at 37 °C. Subsequently, the following experiments were conducted according to the procedure in a previous study. Loss of GSH (%) was calculated as the difference in absorbance between the sample and negative control divided by the absorbance of the negative control. However, material-Ab (1 or 10 μg mL^{-1}) was treated with A431 cells and then subjected to 3 h of incubation at 37 °C in darkness. After incubation, this mixture was photoexcited (with the previously described ROS neutralization); photoexcited with the same treatment; subjected to 3 h of incubation at 37 °C in darkness; and mixed with GSH/bicarbonate buffer in darkness. The signal of the generated $O_2^{\cdot -}$ was obtained as described in the previous calculation. **Hydroxyl peroxide (H_2O_2), hydroxyl radical ($OH^{\cdot}$) and peroxynitrite ($ONOO^-$).** Materials (1 or 10 μg mL^{-1}) were exposed to TPE photoexcitation [4732.80 nJ $pixel^{-1}$; 6 min (number of scans: approximately 52941 scans); Ex: 980 nm]. ROS were neutralized using 30 ppm of antioxidant *α*-tocopherol/methyl linoleate (Sigma-Aldrich, St. Louis, MO, USA) added in darkness. Subsequently, the mixture was mixed with diluted 2′,7′-dichlorodihydrofluorescein diacetate (H_2DCFDA) solution [H_2DCFDA 2.5 μg (Sigma Aldrich Co., USA)+99.5% EtOH (Sigma Aldrich Co., USA) 500 μL, and diluted 1000-fold with 1×PBS to a final volume of 500 mL] and then exposed to TPE photoexcitation. The colorless H_2DCFDA passes through cell membrances and converts itself into 2′,7′-dichlorodihydrofluorescin (DCFH). In the presenceof H_2O_2, $OH\cdot$ and $ONOO^-$, DCFH is oxidized to dichlorodihydrofluorescein (DCF), which emits green fluorescence (Ex/Em: 498/522 nm). A spectrophotometer was employed for measurements. For ROS neutralization, the mixture was mixed with 30 ppm of antioxidant *α*-tocopherol/methyl linoleate (Sigma Aldrich Co., USA) in darkness and exposed to TPE photoexcitation with the same treatment. Data are mean ± standard deviation (n = 6) (**Tables S3-S5**).

Singlet oxygen quantum yield (Φ_Δ) measurement (Kuo et al., 2022)

From previous study, Φ_Δ can be obtained. Φ_Δ measurements were conducted in D_2O at 355 nm, using *meso*-tetra(4-sulfonatophenyl)porphine dihydrochloride (Sigma-Aldrich, St. Louis, MO, USA) as a reference (Φ_Δ= 0.64).

Two-photon imaging (TPI)

5×10^3 A431 cells per well in a 96-well culture plate were for overnight of incubation in the dark at 37°C with 5% CO_2 in air. The materials (delivered dose of material: 3 μg mL^{-1}.) were added to the incubated cells to process the interaction of antibody-antigen for 2.5 h of incubation in the dark at 37°C.

Remove and replace with the new culture medium and repeat for 3 to 5 times to wash out the nonspecific binding. The cells were embedded in a collagen matrix to mimic the 3D epithelium tissue. And the TPI of material-treated-A431 cells were observed using a nonlinear femtosecond laser microscopy optical system under TPE.

And there is no batch to batch variation for the materials in terms of two-photo properties, and two-photon contrast agents. Different optical system has different detection depth. Due to the detection efficiency and the objective we used, the maximal *z* depth we can be observed by this laser optical system is approximately 245 μm. However, 240 μm in the work can show the optimal resolution in the mimic biological specimens.

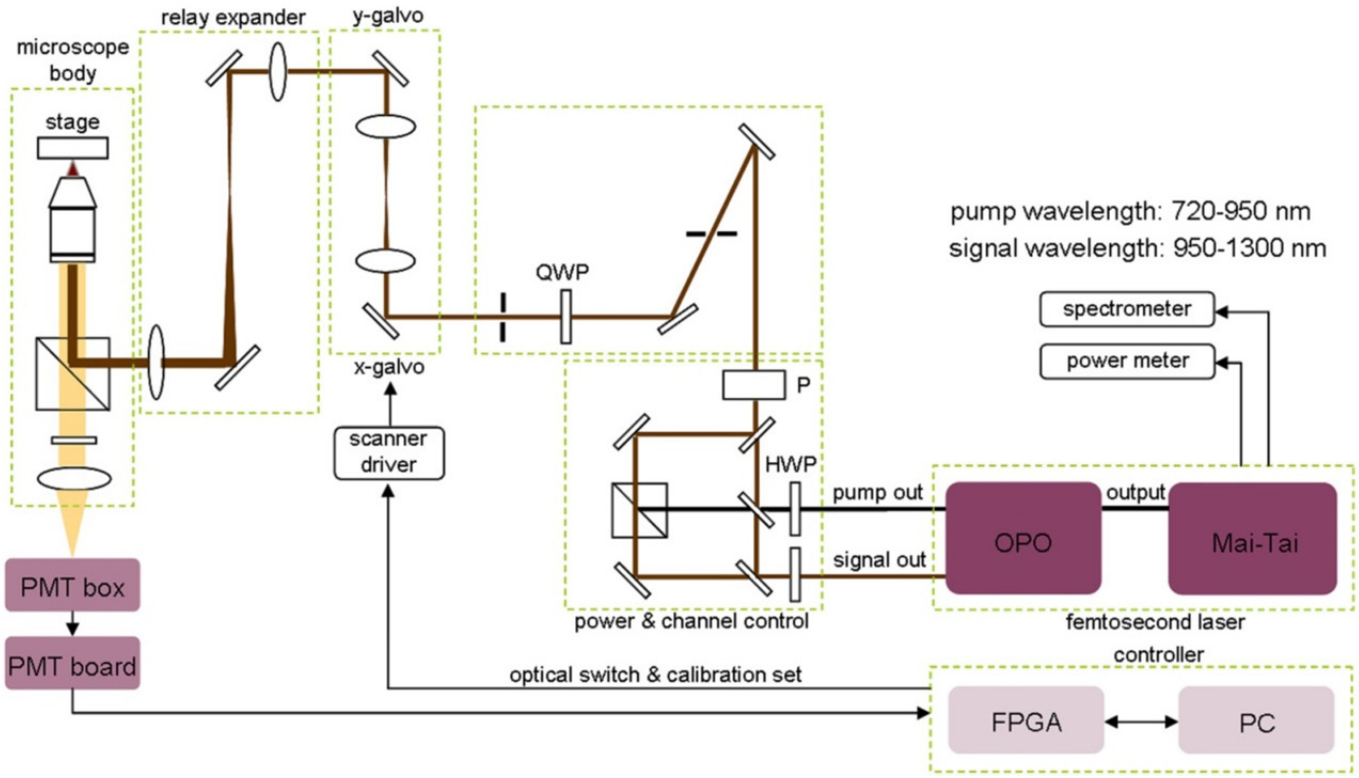

Scheme S1. Layout of the femtosecond laser optical imaging system.

The height profiles of the materials were determined through AFM, and the results indicated a single 1.00 ± 0.03-nm-thick layer of amino-N-GQDs (**Fig. S1a**). FTIR was used to analyze the exposed functional groups of the amino-N-GQDs (**Fig. S1b**). The results showed characteristic bands of amino-N-GQDs for N－H vibration about 891 cm^{-1} (band 1), C－O stretching about 1085 cm^{-1} (band 2), C－N stretching about 1191 cm^{-1} (band 3), tertiary alcoholic C－OH bending about 1392 cm^{-1} (band 4), N－C＝O stretching about 1548 cm^{-1} (band 5), N－H bending about 1637 cm^{-1} (band 6), C＝C ring about 1610 cm^{-1} (band 7), N－H bending and amide about 1759 cm^{-1} (band 8), C＝O stretching about 1832 cm^{-1} (band 9) and N－H vibration about 3295 cm^{-1} (band 10). The results indicated the functional groups of epoxy, hydroxyl, carbonyl, and nitrogen–functionalities groups were exposed from amino-N-GQDs. For the UV-vis absorption spectrum of the amino-N-GQDs, the peaks can be observed. The amino-N-GQDs showed peaks about 225 nm (π-π* transition of aromatic C＝C bonds), and 323 nm (n-π* transition of C–N and C=O shoulder) (**Fig. S1c**). Raman spectroscopy was also used to examine the crystallinity of materials (**Fig. 1c and Fig. S1d**). The major feature bands of amino-N-GQDs are the so-called G bands (~1606 cm^{-1}), which result from the in-plane vibration in a two dimensional hexagonal lattice of sp^2 hybridized C-C bonds; the D band resulted from the defect, disorder, and sp^3-hybridized carbon in graphene layers by breaking the translational symmetry of the lattice occurring at about 1384 cm^{-1}. The results showed that the integrated intensity ratio of the D and G bands (I_D/I_G ratio), which represents the extent of disorder, was 0.90, which is higher than that of graphite (0.104) (**Fig. S1d**), clearly indicating higher distortion of the amino-N-GQDs. This result indirectly indicates that the defect lies within the graphene film having been preferentially attacked for the oxidation to break the starting reduced graphene oxide film into tiny pieces of fewer defects, hence the observed reduced I_D/I_G, indicating the successful conversion from graphite, graphene oxide to amino-N-GQDs. XRD, which was performed to analyze crystallinity, showed the diffraction angle of amino-N-GQDs peaked broadly at about 24.3°, which means an interlayer distance of 0.360 nm (**Figure S1e**). The XRD results suggested that there was no significant basal plane functionalization, which is consistent with our understanding that the graphenes have the much more active edges than the in-plane carbons, as well as the existence of functional groups at the edges of the amino-N-GQDs. The value for one amino-N-GQD is in agreement with values, 0.340–0.403 nm, reported for the amino-N-GQD prepared with other methods (Yeh et al., 2010, Yeh et al., 2014) and the as-prepared amino-N-GQDs were confirmed to have a lamellar, well-ordered structure. The accommodation of various oxygen species, such as epoxy, hydroxyl, carbonyl groups, and changes in the carbon hexahedron grid plane that increase the spacing of the graphene layers result in the increased basal spacing of the amino-N-GQDs (**Fig. S1e**). Full range XPS of the amino-N-GQD, which corresponded to the atomic ratios and bonding compositions of amino-N-GQDs by XPS, was shown in **Fig. S1f**. The conceptual schematic of the amino-N-GQD was shown in **Fig. S1g**.

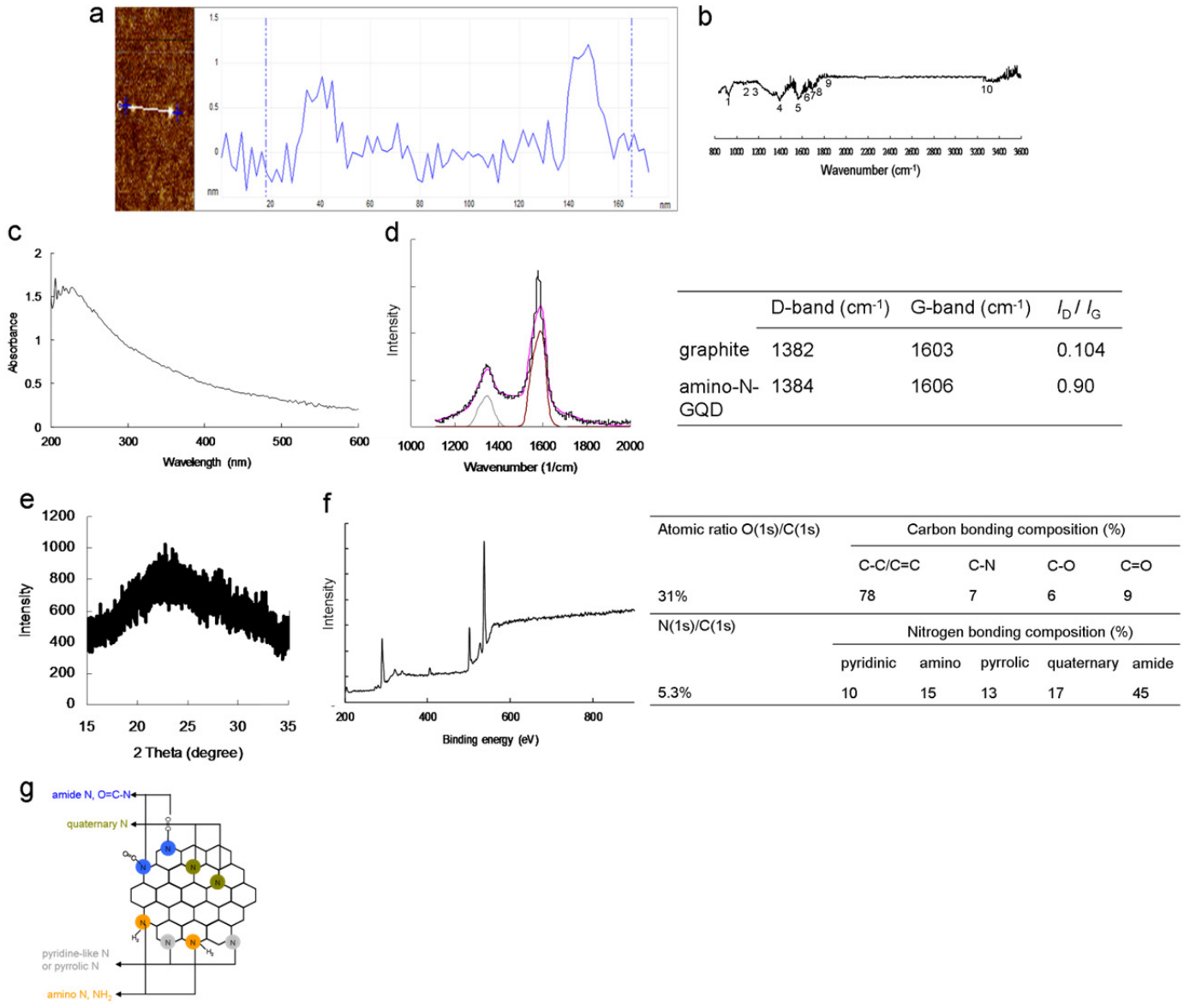

	D-band (cm^{-1})	G-band (cm^{-1})	I_D / I_G
graphite	1382	1603	0.104
amino-N-GQD	1384	1606	0.90

Atomic ratio O(1s)/C(1s)	Carbon bonding composition (%)			
	C-C/C=C	C-N	C-O	C=O
31%	78	7	6	9
N(1s)/C(1s)	**Nitrogen bonding composition (%)**				
	pyridinic	amino	pyrrolic	quaternary	amide
5.3%	10	15	13	17	45

Fig. S1. (a) AFM image of amino-N-GQDs on mica and the height difference between the amino-N-GQD and mica was 1.00 ± 0.03 nm. (b) FTIR spectrum of amino-N-GQDs. (c) UV-Vis, and (d) Raman spectrum of graphite. The gray and brown lines represent the fitted D-band (~1382 cm^{-1}) and G-band (~1603 cm^{-1}) peaks, respectively (black line: raw data; pink line: decomposed spectrum). (e) XRD pattern of amino-N-GQDs. (f) Full range XPS of the amino-N-GQD, which corresponded to the atomic ratios and bonding compositions are summarized and presented as table. And the O(1s)/C(1s) and N(1s)/C(1s) atomic ratios are 31% and 5.3%, respectively. (g) The conceptual schematic of the amino-N-GQD.

Raman spectroscopy was used to monitor the inelastic phonon scattering caused by the vibration of chemical bonds which enables to calculate the size of the sp^2 domain in the amino-N-GQD and amino-N-GQD-PSS-PEI (or amino-N-GQD-polymer composites), respectively. If the mean size of the GQD-based materials > 3 nm, follow the Equation (S10) (Pimenta et al., 2007, Tuinstra et al., 1970),

$$L_a\,(\text{nm}) = (2.4 \times 10^{-10})\,\lambda_{laser}^{4}\,(I_D/I_G)^{-1} \qquad \text{(Equation S10)}$$

where L_a (nm) is the mean size of the sp^2 domain; λ_{Laser} is the excitation wavelength (nm); I means the intensity for the D band and G band, respectively.

However, if the mean size of the GQD-based materials < 3 nm, follow the Equation (S11) (Ferrari et al., 2000),

$$L_D = 0.54\,E_L^{4}\,(I_D/I_G) \qquad \text{(Equation S11)}$$

where is that in small-size graphene sheets with point-like defects containing sp^3-bonded carbon atoms, the mean distance between defects, L_D (nm), is generally used to represent the size of the sp^2 domains L_D, (nm); E_{Laser} is the excitation laser energy (eV) used in Raman experiments.

The Raman spectra were obtained with a 532 nm laser and were decomposed into the D band and G band by the Lorentzian function. According to the calculations based on the Eqs. (S10-S11), the diameter of the amino-N-GQD and amino-N-GQD-polymer composite was 6.9 nm (compared to 7.1 ± 0.6 nm of that determined by HR-TEM) and 7.8 nm due to the conjugation of polymers.

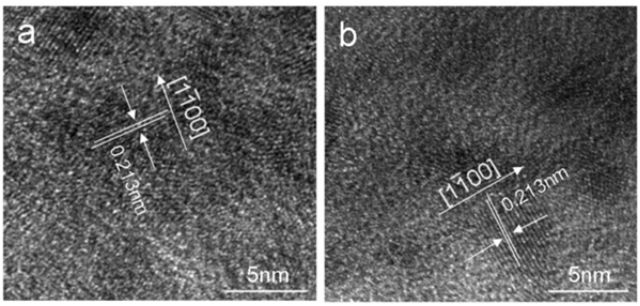

Fig. S2. HR-TEM of (a) amino-N-GQD-PEI and (b) amino-N-GQD-PEI-PSS presented the mean lateral size at approximately 7.5 ± 0.5 nm and 7.9 ± 0.7 nm, respectively. Magnification of the amino-N-GQD-polymer composites revealed that the interlayer spacing of 0.213 nm corresponded to the *d*-spacing of the graphene $\{1\bar{1}00\}$ lattice fringes, indicating the presence of graphene core in amino-N-GQD.

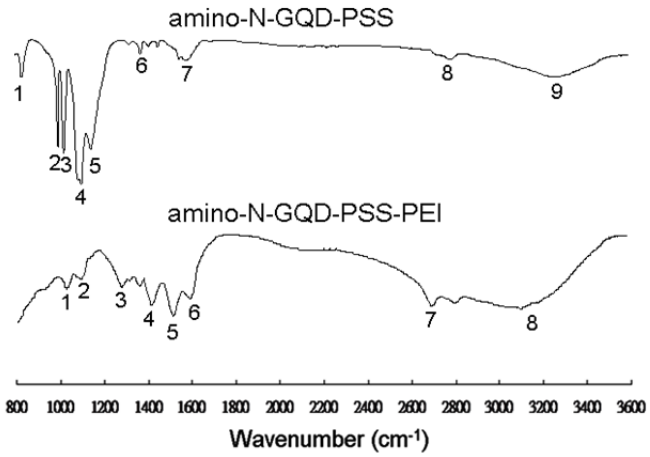

Fig. S3. FTIR spectra of amino-N-GQD-PSS and amino-N-GQD-PSS-PEI (or amino-N-GQD-polymer composites), respectively. Except for the characterization of amino-N-GQDs by FTIR in **Fig. S1b**, results also showed the spectrum of amino-N-GQD-PSS-PEI. The characteristic bands of amino-N-GQD-PSS were approximately for 812 cm^{-1} of C－H bending (band 1), 1019 and 1069 cm^{-1} of in-plane C－H bending (bands 2 and 3), 1141, 1186 and 1409 cm^{-1} of C－H bending (bands 4-6), 1616 cm^{-1} of ring C＝C stretching (band 7), 2722 cm^{-1} of C－H stretching (band 8), and 3250 cm^{-1} of primary sulfonamide (band 8). Besides, the characteristic bands of amino-N-GQD-polymer composites were about for C－N stretching 1018 and 1143 cm^{-1} (bands 1 and 2), for C－H bending 1277 cm^{-1} (band 3), for N－H bending 1401 cm^{-1} (band 4), for N－H bending and scissor 1525 and 1603 cm^{-1} (bands 5 and 6), for C－H stretching 2658 cm^{-1} (band 7), and for N－H stretching 3203 cm^{-1} (band 9), respectively.

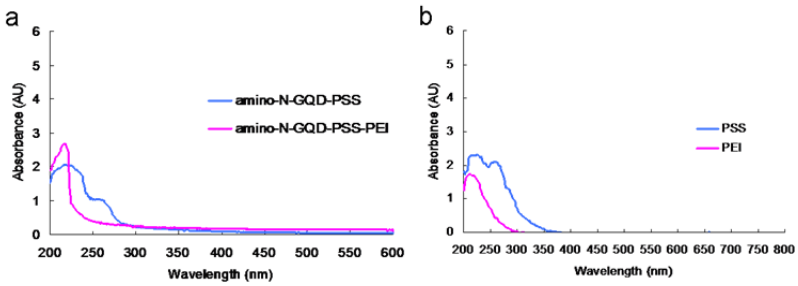

Fig. S4. UV-Vis spectra of (a) amino-N-GQD-PSS, amino-N-GQD-PSS-PEI, and (b) polymers. The amino-N-GQD showed peaks at approximately 225 nm (π-π* transition of aromatic C=C bonds) and 323 nm (n-π* transition of the C=O shoulder and C−N). Amino-N-GQD-PSS exhibited absorptions at approximately 220 and 257 nm due to the coating of PSS. Amino-N-GQD-PSS-PEI (or amino-N-GQD-polymer composites) showed absorption at approximately 219. The broadly characteristic peaks of PSS were shown approximately at 217 nm and 252 nm, respectively, and that of PEI was approximately at 214 nm.

After the conjugation of PSS and PEI, in sequence (amino-N-GQD-PSS-PEI or amino-N-GQD-polymer composites, **Fig. S5**, the position of the D band and G band shift from 1384 to 1355 cm^{-1} and from 1606 to 1589 cm^{-1}, respectively, compared with amino-N-GQD **Fig. 1b**. The I_D/I_G intensity ratio of amino-N-GQD-PSS-PEI was 0.97, respectively. Probably because PSS and PEI are electron-donor molecules that cause high-frequency, tangential, vibrational modes of the carbon molecules in the N-GQD-polymers to shift to lower frequencies (Rao et al., 1997).

The Raman spectra were obtained with a 532 nm laser and were decomposed into the D band and G band by the Lorentzian function. According to the calculations based on the Equations (S10-S11), the diameter of the amino-N-GQD-polymer composites was 7.8 nm due to the conjugation of polymers.

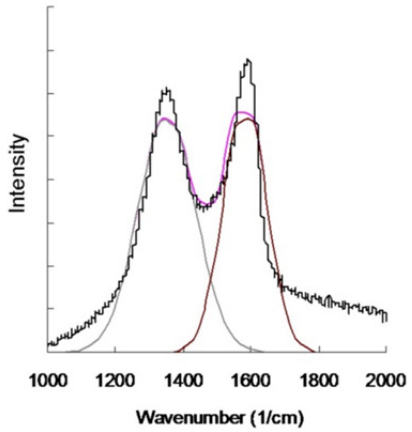

Fig. S5. Raman spectrum of amino-N-GQD-polymer composites. The gray and brown lines represent the fitted D-band (~1355 cm^{-1}) and G-band (~1589 cm^{-1}) peaks, respectively (black line: raw data; pink line: decomposed spectrum).

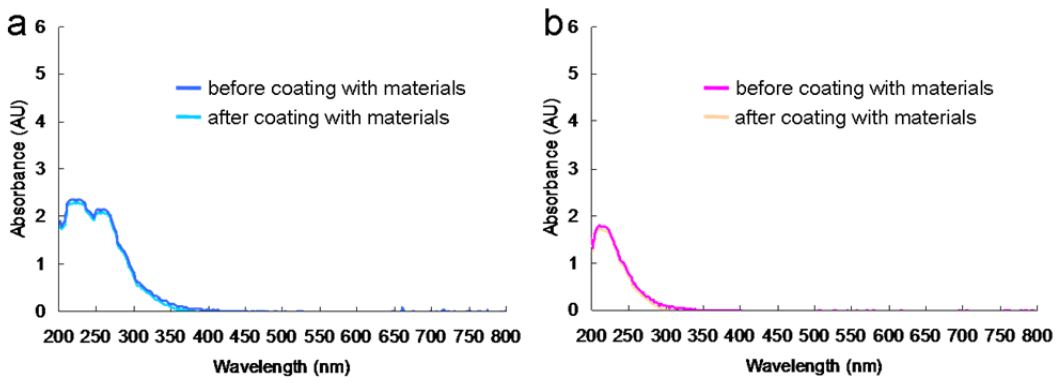

Fig. S6. The absorbance of a quantity of (a) PSS and (b) PEI before/after coating, and spectra were recorded by UV-Vis spectroscopy, respectively (PSS: approximately217 nm and 252 nm; PEI: approximately214 nm).

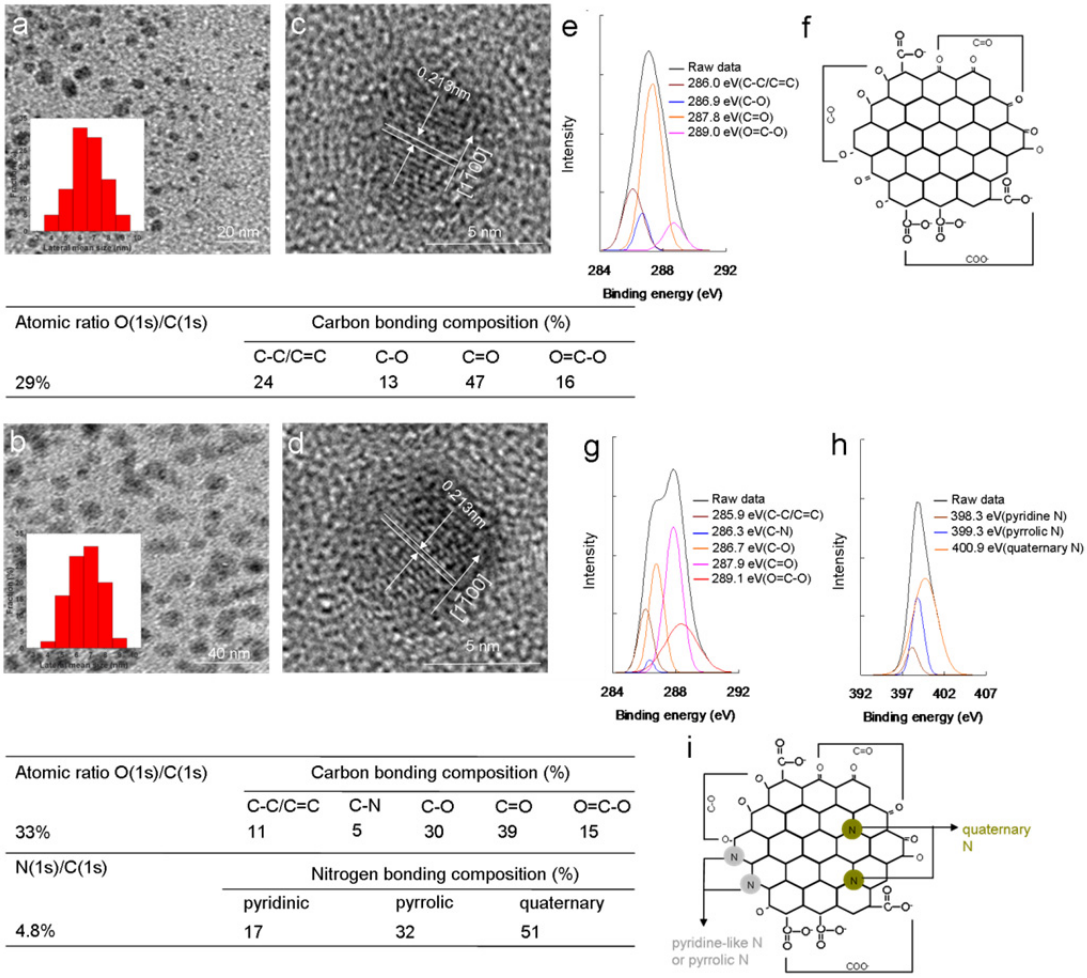

Atomic ratio O(1s)/C(1s)	Carbon bonding composition (%)			
	C-C/C=C	C-O	C=O	O=C-O
29%	24	13	47	16

Atomic ratio O(1s)/C(1s)	Carbon bonding composition (%)				
	C-C/C=C	C-N	C-O	C=O	O=C-O
33%	11	5	30	39	15
N(1s)/C(1s)	Nitrogen bonding composition (%)				
	pyridinic		pyrrolic		quaternary
4.8%	17		32		51

Fig. S7. (a,b) Low-magnified TEM image and (c,d) HR-TEM image captured for a single GQD and N-GQD (mean lateral size = ~7.03 ± 0.5 nm and ~7.10 ± 0.7 nm; interlayer spacing= 0.213 nm), respectively. (e) The deconvoluted carbon C(1s) spectra of GQD were from C−C/C=C (286.0 eV), C−O (286.9 eV), C=O (287.8 eV) and O=C−O (289.0 eV), respectively. The C(1s) spectrum of GQD showed the O(1s)/C(1s) ratio to be about 29%. The relevant table summarizes the bonding composition and atomic ratio of the GQDs. (f) Conceptual schematic of the GQD. (g) The deconvoluted carbon C(1s) spectra of N-GQD were from C−C/C=C (285.9 eV), C−N (286.3 eV), C−O (286.7 eV), C=O (287.9 eV), and O=C−O (289.1 eV), respectively; the deconvoluted N(1s) spectra of N-GQD were pyridinic–N (398.3 eV), pyrrolic–N (399.3 eV), and quaternary–N (400.9 eV), respectively. The C(1s) and N(1s) spectrum of N-GQD showed the O(1s)/C(1s) and N(1s)/C(1s) ratios to be about 33% and 4.8%. The relevant table summarizes the bonding composition and atomic ratio of the N-GQDs. (i) Conceptual schematic of the N-GQD.

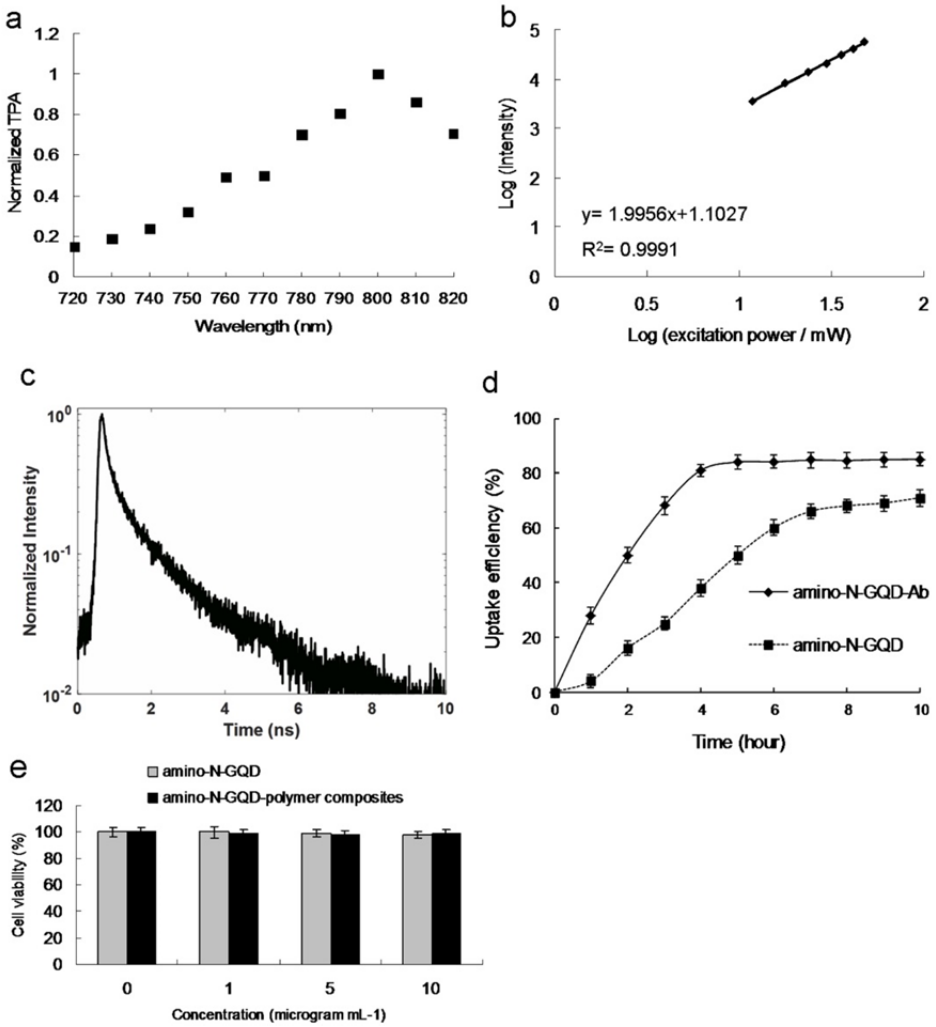

Fig. S8. (a) Relative TPA spectra of the amino-N-GQD. TPE with a function of the wavelength (900-1000 nm) at 118.32 nJ pixel^{-1} that was used to monitor the signals. (b) TPL intensity dependence on the excitation power (logarithm) of the amino-N-GQD with slope of approximately 1.99, exposed from 1183.20 (11.832 mW) to 4732.80 nJ pixel^{-1} (47.328 mW) of TPE. $R^2 > 0.999$ (Ex: 980 nm). (c) Time-resolved PL decay profiles of materials monitored at room temperature (Ex: 980 nm, 118.32 nJ pixel^{-1}). (d) Uptake assays of amino-N-GQD-Ab$_{EGFR}$- and amino-N-GQD-polymer composites-Ab$_{EGFR}$-treated A431 skin cancer cells for 0–10 h at 37 °C. Delivered dose of material: 1 μg mL^{-1}. (e) A431 skin cancer cells were incubated with materials (0-10 μg mL^{-1}) in the dark for 24 h and then their viability was evaluated by MTT assay. Data are means ± SD (n = 6).

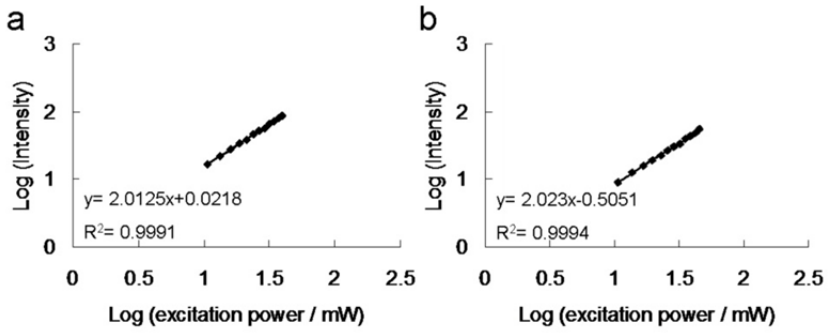

Fig. S9. Logarithmic plat of TPL intensity as a function of TPE from 1183.2 nJ pixel^{-1} to 4732.8 nJ pixel^{-1}. (a) Fluorescein (in ddH_2O, pH 11) with a slope of approximately 2.01 and (b) Rhodamine B (in methanol) with a slope of approximately 2.02. $R^2 > 0.99$. Excitation wavelength: 980 nm.

Table S1. Two-photon action cross sections of fluorescein (in 0.1 M NaOH, pH 11) and rhodamine B (in methanol). Excitation wavelength: 980 nm.

	Fluorescein (in ddH_2O, pH=11)	Rhodamine B (in methanol)
Excitation wavelength at 980 nm action cross section, $\eta\ \sigma_2$ (GM, $10^{-50}cm^4s$/photon)	15.83	20.01

Table S2. Stability of materials in physiological environments was determined by DLS.

	Mean lateral size (nm)		
	ddH_2O	PBS	culture medium for A431 cells
amino-N-GQD	7.3 ± 0.3	7.4 ± 0.5	7.5 ± 0.4
amino-N-GQD-polymer composites	7.9 ± 0.4	7.9 ± 0.5	7.9 ± 0.7

Table S3. Generated ROS determined through TPE [power: 4732.80 nJ pixel^{-1}; 6 min (number of scans: approximately 52941 scans); Ex: 980 nm] with material (1 or 10 μg mL^{-1}). Data are means ± SD (n = 6) (Kinen et al., 2000, Kuo et al., 2009, Kuo et al., 2016, Kuo et al., 2017, Possel et al., 1997).

	$^1O_2$ (by SOSG)[c]						
	Negative control[ac]	ROS neutralization[abc]	Positive control[cd]	amino-N-GQD	ROS neutralization[bc]	amino-N-GQD-PSS-PEI	ROS neutralization[bc]
1 μg mL^{-1}	205±11	204±10	2275±123	2048±110	205±10	208±10	205±9
10 μg mL^{-1}	207±12	205±10	4104±165	4001±158	206±11	209±11	205±12
	$^1O_2$ (by *t*-MVP)[e]						
	Negative control[ae]	ROS neutralization[abe]	Positive Control[de]	amino-N-GQD	ROS neutralization[be]	amino-N-GQD-PSS-PEI	ROS neutralization[be]
1 μg mL^{-1}	321±12	320±11	7015±188	6460±171	322±11	325±9	322±10
10 μg mL^{-1}	321±13	319±13	16229±290	15414±263	323±12	325±11	324±10
	$O_2 \bullet^-$ (by XTT)[f]						
	Negative control[af]	ROS neutralization[abf]	Positive Control[df]	amino-N-GQD	ROS neutralization[bf]	amino-N-GQD-PSS-PEI	ROS neutralization[bf]
1 μg mL^{-1}	0	0	1.45±0.14	1.30±0.12	0.03±0.01	0.04±0.01	0.03±0.01
10 μg mL^{-1}	0	0	3.11±0.25	2.98±0.19	0.03±0.01	0.03±0.01	0.03±0.02
	$O_2 \bullet^-$ (by GSH)[g]						
	Negative control[ag]	ROS neutralization[abg]	Positive control[dg]	amino-N-GQD	ROS neutralization[bg]	amino-N-GQD-PSS-PEI	ROS neutralization[bg]
1 μg mL^{-1}	0	0	97.0±2.1%	89.4±1.5%	0.4±0.1%	0.6±0.1%	0.3±0.1%
10 μg mL^{-1}	0	0	99.9±2.5%	95.6±2.0%	0.4±0.2%	0.5±0.1%	0.3±0.1%
	H_2O_2, OH^-, $ONOO^-$ (by H_2DCFDA)[h]						
	Negative control[ah]	ROS neutralization[abh]	Positive control[dh]	amino-N-GQD	ROS neutralization[bh]	amino-N-GQD-PSS-PEI	ROS neutralization[bh]
1 μg mL^{-1}	70±5	71±5	2041±88	101±13	69±3	70±2	71±6
10 μg mL^{-1}	72±6	70±3	3115±106	169±20	71±7	70±3	72±4

[a]Negative control: only reagent and laser irradiation were used without material (0 μg mL^{-1}).

[b]ROS neutralization: the process involved material treatments, laser irradiation, and treatment with 30 ppm of antioxidant α-tocopherol/methyl linoleate.

[c]The SOSG reagent (Ex/Em: 488/525 nm) has a suitable specific reactivity for generating fluorescence, which was recorded using a spectrophotometer.

[d]Positive control: treatment with 50 μM *tert*-butyl hydroperoxide and laser irradiation were performed.

[e]*t*-MVP (Ex/Em: 352/465 nm) reacted with $^1O_2$ and formed a dioxetane intermediate, which generated fluorescence upon decomposition into 1-pyrenecarboxaldehyde. This process was monitored using a

spectrophotometer.

[f]XTT interacted with $O_2^{\cdot -}$ and produced XTT-formazan, which generated strong absorption (wavelength: 470 nm).

[g]GSH containing a thiol-tripeptide can prevent damage to cellular or bacterial components caused by oxidative stress. This thiol group from GSH was oxidized to disulfide; thus, GSH was converted into resulting in glutathoine disulfide. GSH oxidation was used to determine the generated $O_2^{\cdot -}$. Loss of GSH (%) = (absorbance difference between sample and negative control/absorbance of negative control) × 100%.

[h]H_2DCFDA passes through cell membranes and converts itself into DCFH. In the presenceof H_2O_2, OH· and $ONOO^-$, DCFH is oxidized to DCF, which emits green fluorescence (Ex/Em: 498/522 nm). A spectrophotometer was employed for measurements.

Table S4. Generated ROS determined through TPE [power: 4732.80 nJ pixel^{-1}; 6 min (number of scans: approximately 52941 scans); Ex: 980 nm] on A431 cells treated with material (1 or 10 μg mL^{-1})-Ab$_{EGFR}$. Data presented as means ± SD (n = 6) (Kinen et al., 2000, Kuo et al., 2009, Kuo et al., 2016, Kuo et al., 2017, Possel et al., 1997).

	$^1O_2$ (by SOSG)[c]						
	Negative control[ac]	ROS neutralization[abc]	Positive control[cd]	amino-N-GQD	ROS neutralization[bc]	amino-N-GQD-PSS-PEI	ROS neutralization[bc]
1 μg mL^{-1}	204±9	205±10	2263±124	1795±102	205±9	206±10	204±9
10 μg mL^{-1}	206±10	205±11	4018±161	3832±149	206±11	207±10	205±11
	$^1O_2$ (by *t*-MVP)[e]						
	Negative control[ae]	ROS neutralization[abe]	Positive control[de]	amino-N-GQD	ROS neutralization[be]	amino-N-GQD-PSS-PEI	ROS neutralization[be]
1 μg mL^{-1}	319±14	318±12	6930±182	5577±140	320±9	322±12	319±10
10 μg mL^{-1}	320±14	320±16	15842±285	14199±287	321±11	323±12	320±11
	$O_2 \bullet^-$ (by XTT)[f]						
	Negative control[af]	ROS neutralization[abf]	Positive Control[df]	amino-N-GQD	ROS neutralization[bf]	amino-N-GQD-PSS-PEI	ROS neutralization[bf]
1 μg mL^{-1}	0	0	1.41±0.12	1.22±0.11	0.03±0.02	0.04±0.01	0.03±0.01
10 μg mL^{-1}	0	0	3.07±0.26	2.85±0.20	0.03±0.01	0.03±0.01	0.03±0.02
	$O_2 \bullet^-$ (by GSH)[g]						
	Negative control[ag]	ROS neutralization[abg]	Positive control[dg]	amino-N-GQD	ROS neutralization[bg]	amino-N-GQD-PSS-PEI	ROS neutralization[bg]
1 μg mL^{-1}	0	0	96.5±1.8%	86.3±1.2%	0.4±0.1%	0.5±0.1%	0.4±0.1%
10 μg mL^{-1}	0	0	99.9±2.4%	93.9±2.6%	0.4±0.2%	0.6±0.2%	0.3±0.1%
	H_2O_2, OH^-, $ONOO^-$ (by H_2DCFDA)[h]						
	Negative control[ah]	ROS neutralization[abh]	Positive control[dh]	amino-N-GQD	ROS neutralization[bh]	amino-N-GQD-PSS-PEI	ROS neutralization[bh]
1 μg mL^{-1}	72±4	70±4	2069±91	89±10	72±4	71±3	70±5
10 μg mL^{-1}	71±5	72±2	3140±112	154±17	72±6	72±4	71±5

[a]Negative control: only reagent and laser irradiation were used without material (0 μg mL^{-1}).

[b]ROS neutralization: the process involved material treatments, laser irradiation, and treatment with 30 ppm of antioxidant α-tocopherol/methyl linoleate.

[c]The SOSG reagent (Ex/Em: 488/525 nm) has a suitable specific reactivity for generating fluorescence, which was recorded using a spectrophotometer.

[d]Positive control: treatment with 50 μM *tert*-butyl hydroperoxide and laser irradiation were performed.

[e]*t*-MVP (Ex/Em: 352/465 nm) reacted with $^1O_2$ and formed a dioxetane intermediate, which generated

fluorescence upon decomposition into 1-pyrenecarboxaldehyde. This process was monitored using a spectrophotometer.

[f]XTT interacted with $O_2^{\cdot -}$ and produced XTT-formazan, which generated strong absorption (wavelength: 470 nm).

[g]GSH containing a thiol-tripeptide can prevent damage to cellular or bacterial components caused by oxidative stress. This thiol group from GSH was oxidized to disulfide; thus, GSH was converted into resulting in glutathoine disulfide. GSH oxidation was used to determine the generated $O_2^{\cdot -}$. Loss of GSH (%) = (absorbance difference between sample and negative control/absorbance of negative control) × 100%.

[h]H_2DCFDA passes through cell membranes and converts itself into DCFH. In the presenceof H_2O_2, OH· and $ONOO^-$, DCFH is oxidized to DCF, which emits green fluorescence (Ex/Em: 498/522 nm). A spectrophotometer was employed for measurements.

Table S5. Generated ROS determined through TPE [power: 4732.80 nJ pixel^{-1}; 6 min (number of scans: approximately 52941 scans); Ex: 980 nm] on A431 cells treated with material (1 or 10 μg mL^{-1}). Data are means ± SD (n = 6) (Kinen et al., 2000, Kuo et al., 2009, Kuo et al., 2016, Kuo et al., 2017, Possel et al., 1997).

	$^1O_2$ (by SOSG)[c]						
	Negative control[ac]	ROS neutralization[abc]	Positive control[cd]	amino-N-GQD	ROS neutralization[bc]	amino-N-GQD-PSS-PEI	ROS neutralization[bc]
1 μg mL^{-1}	204±11	205±11	2199±120	1246±78	206±9	207±11	206±11
10 μg mL^{-1}	205±12	206±12	3988±156	3543±141	207±10	208±11	207±9

	$^1O_2$ (by *t*-MVP)[e]						
	Negative control[ae]	ROS neutralization[abe]	Positive control[de]	amino-N-GQD	ROS neutralization[be]	amino-N-GQD-PSS-PEI	ROS neutralization[be]
1 μg mL^{-1}	318±13	320±14	6874±177	4169±132	319±15	322±12	320±14
10 μg mL^{-1}	319±15	320±15	15602±274	12835±200	320±14	323±14	322±16

	$O_2 \bullet^-$ (by XTT)[f]						
	Negative control[af]	ROS neutralization[abf]	Positive control[df]	amino-N-GQD	ROS neutralization[bf]	amino-N-GQD-PSS-PEI	ROS neutralization[bf]
1 μg mL^{-1}	0	0	1.45±0.14	1.01±0.06	0.02±0.01	0.04±0.01	0.03±0.01
10 μg mL^{-1}	0	0	3.03±0.24	2.59±0.19	0.02±0.01	0.04±0.01	0.02±0.01

	$O_2 \bullet^-$ (by GSH)[g]						
	Negative control[ag]	ROS neutralization[abg]	Positive control[dg]	amino-N-GQD	ROS neutralization[bg]	amino-N-GQD-PSS-PEI	ROS neutralization[bg]
1 μg mL^{-1}	0	0	96.9±1.9%	79.4±0.8%	0.3±0.1%	0.4±0.1%	0.3±0.2%
10 μg mL^{-1}	0	0	99.9±2.3%	88.1±1.1%	0.3±0.1%	0.4±0.2%	0.3±0.1%

	H_2O_2, OH^-, $ONOO^-$ (by H_2DCFDA)[h]						
	Negative control[ah]	ROS neutralization[abh]	Positive control[dh]	amino-N-GQD	ROS neutralization[bh]	amino-N-GQD-PSS-PEI	ROS neutralization[bh]
1 μg mL^{-1}	73±3	71±5	2060±89	81±10	71±5	70±4	71±3
10 μg mL^{-1}	72±5	73±4	3114±108	146±13	71±7	72±2	72±4

[a]Negative control: only reagent and laser irradiation were used without material (0 μg mL^{-1}).

[b]ROS neutralization: the process involved material treatments, laser irradiation, and treatment with 30 ppm of antioxidant α-tocopherol/methyl linoleate.

[c]The SOSG reagent (Ex/Em: 488/525 nm) has a suitable specific reactivity for generating fluorescence, which was recorded using a spectrophotometer.

[d]Positive control: treatment with 50 μM *tert*-butyl hydroperoxide and laser irradiation were performed.

[e]*t*-MVP (Ex/Em: 352/465 nm) reacted with $^1O_2$ and formed a dioxetane intermediate, which generated fluorescence upon decomposition into 1-pyrenecarboxaldehyde. This process was monitored using a spectrophotometer.

[f]XTT interacted with $O_2^{\cdot-}$ and produced XTT-formazan, which generated strong absorption (wavelength: 470 nm).

[g]GSH containing a thiol-tripeptide can prevent damage to cellular or bacterial components caused by oxidative stress. This thiol group from GSH was oxidized to disulfide; thus, GSH was converted into resulting in glutathoine disulfide. GSH oxidation was used to determine the generated $O_2^{\cdot-}$. Loss of GSH (%) = (absorbance difference between sample and negative control/absorbance of negative control) × 100%.

[h]H_2DCFDA passes through cell membranes and converts itself into DCFH. In the presenceof H_2O_2, OH· and $ONOO^-$, DCFH is oxidized to DCF, which emits green fluorescence (Ex/Em: 498/522 nm). A spectrophotometer was employed for measurements.

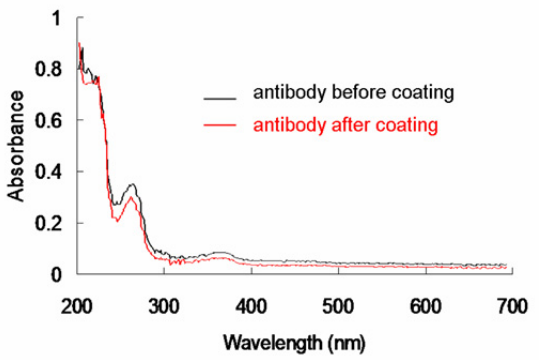

Fig. S10. The absorbance of a quantity of antibody before/after coating, and spectra were recorded by UV-Vis spectroscopy, respectively (Abs: approximately 216 nm and 272 nm).

Table S6. Material TPE cross section (Ex: 980 nm).

Reference	Integrated emission intensity (counts)		Action cross-section (ησ)
Fluorescein[a]	55.17		15.83
Sample	**Integrated emission intensity (counts)**	**Relative quantum yield (η)**	**Absolute cross-section (σ)**
amino-N-GQD	50471.98	0.28	51721.40
amino-N-GQD-polymer composites	133011.49	0.63	60579.62

[a]Fluorescein was selected as the standard reference for the cross section, and the relevant calculations are presented in the materials and methods section.

References

Ferrari, A.C., Basko, D.M., 2013. Raman spectroscopy as a versatile tool for studying the properties of graphene, Nat. Nanotechnol. 8 (4), 235–246. http://doi.org/10.1038/nnano.2013.46

Ferrari, A.C., Robertson, J., 2000. Interpretation of Raman spectra of disordered and amorphous carbon, Phys. Rev. B 61, 14095–14107. https://doi.org/10.1103/PhysRevB.61.14095

Horton, N.G., Wang, K., Kobat, D., Clark, C.G., Wise, F.W., Schaffer, C.B., Xu, C., 2013. In vivo three-photon microscopy of subcortical structures within an intact mouse brain. Nat. Photonics 7 (3), 205–209. https://doi.org/ 10.1038/nphoton.2012.336

Hummers, W.S., Offeman, R.E., 1958. Preparation of graphitic oxide. J. Am. Chem. Soc. 80 (6), 1339. https://doi.org/10.1021/ja01539a017

Kinen, M.M., Kamal-Eldin, A., Lampi, A.M., Hopia, A., 2000. Effects of α- and γ- tocopherols on formation of hydroperoxides and two decomposition products from methyl linoleate, J. Am. Oil Chem. Soc. 77, 801–806. https://doi.org/10.1016/10.1007/s11746-000-0128-z

Kuo, W.S., Chang, C.N., Chang, Y.T., Yeh, C.S., 2009 Antimicrobial gold nanorods dual-modality photodynamic therpay inactivation and hyperthermia, Chem. Commun. (32), 4853−4855. https://doi.org/10.1039/b907274h

Kuo, W.S., Chang, C.Y., Chen, H.H., Hsu, C.L.L., Wang, J.Y., Kao, H.F., Chou, L.C.S., Chen, Y.C., Chen, S.J., Chang, W.T., Tseng, S.W., Wu, P.C., Pu, Y.C., 2016. Two-photon photoexcited photodynamic therapy and contrast agent with antimicrobial graphene quantum dots. ACS Appl. Mater. Interfaces 8 (44), 30467–30474. https://doi.org/10.1021/acsami.6b12014

Kuo, W.S., Chen, H.H., Chen, S.Y., Chang, C.Y., Chen, P.C., Hou, Y.I., Shao, Y.T., Kao, H.F., Hsu, C.L L., Chen, Y.C., Chen, S.J., Wu, S.R., Wang, J.Y., 2017. Graphene quantum dots with nitrogen-doped content dependence for highly efficient dual-modality photodynamic antimicrobial therapy and bioimaging. Biomaterials 120, 185–194. https://doi.org/10.1016/j.biomaterials.2016.12.022

Kuo, W.S., Lien, C.H., Cho, K.C., Chang, C.Y., Lin, C.Y., Huang, L.L.H., Campagnola, P.J., Dang, C.Y., Chen, S.J., 2010. Multiphoton fabrication of freeform polymer microstructures with gold nanorods. Opt. Express 18 (26), 27550–27559. https://doi.org/10.1364/OE.18.027550

Kuo, W.S., Wu, P.C., Chang, C.Y., Chang, C.Y., Wang, J.Y., Chen, P.C., Hsieh, M.S., Lin, S.H., Cheng, J.S., Chou Y.T., 2022. Graphene near infrared-I/II probe in two-photon excitation-wavelength-independent photoluminescence and photoinactivation. Carbon 193, 205–215. https://doi.org/10.1016/j.carbon.2022.03.019

Li, B., Wu, C., Wang, M., Charan, K., Xu, C., 2020. An adaptive excitation source for high-speed multiphoton Microscopy. Nat. Methods 17 (2), 163–166. https://doi.org/10.1038/s41592-019-0663-9

Lakowicz. J.R., 2006. Principles of fluorescence spectroscopy, third ed. Springer US, Baltimore, pp. 1−26.

Li, Y., Zhao, T., Cheng, H., Hu, Y., Shi, G., Dai, L., Qu, L., 2012. Nitrogen-doped graphene quantum dots with oxygen-rich functional groups. J. Am. Chem. Soc. 134 (1), 15–18. http://doi.org/10.1021/ja206030c

Ouzounov, D.G., Wang, T., Wang, M., Feng, D.D., Horton, N.G., Cruz-Hernández, J.C., Cheng, Y.T., Reimer, J., Tolias, A.S., Nishimura, N., Xu, C., 2017. In vivo three-photon imaging of activity of GCaMP6-labeled neurons deep in intact mouse brain. Nat. Methods 14 (4), 388–390. https://doi.org/10.1038/nmeth.4183

Pimenta, M.A., Dresselhaus, G., Dresselhaus, M.S., Cancado, L.G., Jorio, A., Saito, R., 2007. Studying disorder in graphite-based systems by Raman spectroscopy, Phys. Chem. Chem. Phys. 9 (11), 1276–1290. https://doi.org/10.1039/b613962k

Possel, H., Noack, H., Augustin, W., Keilhoff, G., Wolf, G., 1997. An oxidant, *tert*-butyl hydroperoxide (TBHP), to serve as a positive control. FEBS Lett. 416, 175–178

Rao, A.M., Eklund, P.C., Banbow, S., Thess, A., Smalley, R.E., 1997. Diameter-selective Raman scattering from vibrational modes in carbon nanotubes, Science 275 (5297) 187–191. https://doi.org/ 10.1126/science.275.5297.187

Suhling, K., Hirvonen, L.M., Levitt, J.A., Chung, P.H., Tregido, C., Le Marois, A., Rusakov, D.A., Zheng, K., Ameer-Beg, S., Poland, S., Coelho, S., Henderson, R., Krstajic, N., 2015. Fluorescence lifetime imaging (FLIM): basic concepts and recent developments. Medical Photonics 27, 3–40. https://doi.org/10.1016/j.medpho.2014.12.001

Tuinstra, F., Koenig, J.L., 1970. Raman spectrum of graphite, J. Phys. Chem. 53, 1126–1130. https://doi.org/10.1063/1.1674108

Umezawa, K., Matsui, A., Nakamura, Y., Citterio, D., Suzuki, K., 2009. Bright, color-tunable fluorescent dyes in the Vis/NIR region: establishment of new “tailor-made’ multicolor fluorophores based on borondipyrromethene. Chem. Eur. J. 15 (5), 1096–1106. https://doi.org/10.1002/chem.200801906

Wang, H., Huff, T.B., Zweifel, D.A., He, W., Low, P.S., Wei, A., Cheng, J.X., 2005. In vitro and in vivo two-photon luminescence imaging of single gold nanorods, Proc. Natl. Acad. Sci. USA 102 (44) 15752–15756. https://doi.org/ 10.1073/pnas.0504892102

Xu, C., Zipfel, W., Shear, J.B., Williams, R.M.,Webb, W.W., 1996. Multiphoton fluorescence excitation: new spectral windows for biological nonlinear microscopy. Proc. Natl. Acad. Sci. USA 93 (20), 10763−10768. https://doi.org/10.1073/pnas.93.20.10763

Yeh, T.F., Syu, J.M., Cheng, C., Chang, T.H., Teng, H., 2010. Graphite oxide as a photocatalyst for hydrogen production from water. Adv. Funct. Mater. 20, 2255−2262.

Yeh, T.F., Teng, C.Y., Chen, S.J., Teng, H., 2014. Nitrogen-doped graphene oxide quantum dots as photocatalysts for overall water-splitting under visible light illumination. Adv. Mater. 26, 3297−3303.